IEEE Access
Multidisciplinary | Rapid Review | Open Access Journal

Received November 9, 2021, accepted November 22, 2021, date of publication December 1, 2021,
date of current version December 20, 2021.

Digital Object Identifier 10.1109/ACCESS.2021.3132097

Millimeter-Wave and Terahertz Fixed Wireless Link Budget Evaluation for Extreme Weather Conditions

ZU-KAI WENG[1], ATSUSHI KANNO[2], (Member, IEEE), PHAM TIEN DAT[2], (Member, IEEE), KEIZO INAGAKI[1,2], KOSUKE TANABE[3], EISAKU SASAKI[3], (Member, IEEE), THOMAS KÜRNER[4], BO KUM JUNG[4], AND TETSUYA KAWANISHI[1,2], (Fellow, IEEE)

[1]Department of Electronic and Physical Systems, Faculty of Science and Engineering, Waseda University, Tokyo 169-8555, Japan
[2]National Institute of Information and Communications Technology, Koganei 184-8795, Japan
[3]NEC Corporation, Kawasaki, Kanagawa 211-8666, Japan
[4]Institute for Communications Technology, Technische Universität Braunschweig, 38102 Braunschweig, Germany

Corresponding author: Zu-Kai Weng (weng_zukai@asagi.waseda.jp)

This work was supported by the Waseda Research Institute for Science and Engineering.

ABSTRACT To develop highly reliable fixed wireless links, such as mobile backhaul and fronthaul systems, it is essential to evaluate the link budget under extreme weather conditions. In this paper, we presented a link budget evaluation for fixed wireless links using radio signals at four different carrier frequencies: 75.375, 85.375, 275, and 400 GHz. As examples of extreme weather conditions, we focused on storms which can be defined as the combination of high temperature, violent rain, and strong winds. A theoretical model was proposed to evaluate the attenuation by the wind effect, which was due to mechanical vibration. Using the proposed model, we evaluated the link attenuation with different weather parameters, such as clear weather condition, different rain rates, and strong wind. In addition, the maximum channel capacities were estimated based on the model. According to the calculation results, it can be confirmed that the attenuation caused by heavy rain is the dominant factor to the whole system. Besides, the attenuation due to antenna gain degradation induced by the wind effect is considerable for the wireless link at high frequencies (275 and 400 GHz). This manuscript includes a comprehensive discussion regarding various weather factors including gas, rain, and wind, which impact the fixed wireless links. The obtained results would be useful for designing a high reliability fixed wireless link to operate under different weather conditions.

INDEX TERMS Terahertz (THz), 6G, fixed wireless link, millimeter wave, link budget, attenuation.

I. INTRODUCTION

Today, the development of novel technologies, such as wearable communication, virtual and augmented reality applications, and self-driving automobiles, is fueling the rapid evolution of wireless communications worldwide. Besides, as the coronavirus disease 2019 (COVID-19) pandemic persists, the high dependence on telework, online meetings, and remote lectures has cemented the importance of wireless communications. This has further increased the demand for wireless links with low power consumption and high capacity despite the currently ongoing roll out of the 5th generation (5G) wireless systems [1]–[4]. However, the microwave bands currently used for 5G applications (such as ultrareliable and low-latency services, massive Internet of things) are insufficient for meeting the rapidly rising. In this scenario, research on the 6th generation (6G) of wireless systems has been proposed [5]–[8]. The 6G wireless network is intended to use wireless access in the millimeter-wave (mm-wave) and terahertz (THz) bands, minimize cell sizes, and incorporate photonic network [9]–[11]. In particular, the use of THz carrier frequencies has the potential to considerably increase the channel capacity. Compared with the microwave band, the mm-wave and THz frequency bands have the following three characteristics. First, the available bandwidths are much wider, enabling high-speed transmission and high-precision sensing. Second, the wavelengths are shorter, resulting in an increase in the path loss. However,

The associate editor coordinating the review of this manuscript and approving it for publication was Khmaies Ouahada.

This work is licensed under a Creative Commons Attribution 4.0 License. For more information, see https://creativecommons.org/licenses/by/4.0/

because of its small wavelength, the radio wave can be easily focused within a narrow beam, which makes it easier to build high-gain antennas to mitigate the high path loss, especially for fixed point-to-point applications. In 2017, IEEE published the IEEE Std. 802.15.3d-2017 [12], which targets the application of THz waves for point-to-point wireless communications. One of the scenarios envisioned in this standard and the 6G standard use wireless backhaul links where the conventional cable-based communication channels between base stations and the core network are substituted by wireless links in the THz band [13]–[16]. Nevertheless, the high attenuation and loss of the THz links make long-distance transmission difficult. To assess the feasibility of the mm-wave and THz waves for backhaul/fronthaul applications, which require a transmission distance of up to several hundreds of meters, it is necessary to evaluate the attenuation and link budget of the mm-wave and THz links. Fig. 1 illustrates the attenuation rates of the mm-waves and THz waves in standard air. Although some attenuation peaks can be observed in the THz bands, the attenuation windows between these peaks can be utilized for wireless communications. In the mm-wave band, the frequency bands between 71–76 GHz and 81–86 GHz (blue bands in Fig. 1) are two bands that can be licensed for commercial usage. As mentioned in the APT-AWG-REP-81 [17], 75.375 and 85.375 GHz carriers are two candidates within these bands. At the World Radiocommunication Conference 2019 (WRC-19) [18], four bands in the THz region were identified for fixed and mobile wireless links. These bands are noted in Fig. 1 in green: 275–296 GHz (21 GHz wide), 306–313 GHz (7 GHz wide), 318–333 GHz (15 GHz wide), and 356–450 GHz (94 GHz wide). Together with the already allocated spectrum between 252 and 275 GHz, a total of 160 GHz is now available in the frequency range of 252 to 450 GHz [19].

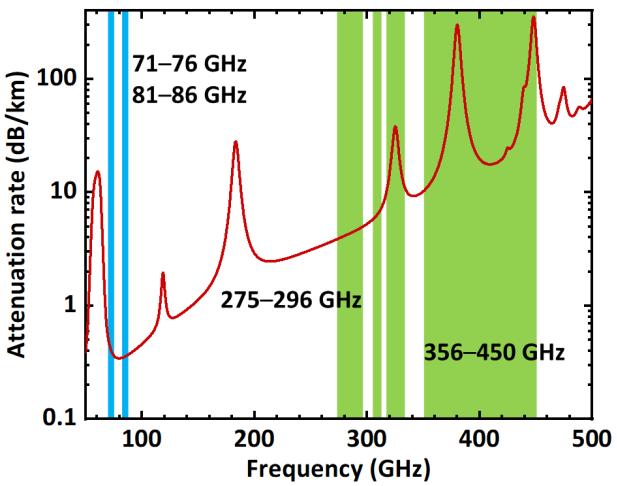

FIGURE 1. Attenuation rate of mm- and THz waves in standard air.

The link budget for millimeter or THz waves based wireless links has been evaluated in previous studies [20]–[22]. For the weather issue, Schneider *et al.* [23] investigated the link budget for THz fixed wireless links considering rain and fog attenuation. Regarding the rain-induced attenuation effect, Fang *et al.* [24] developed an algorithm for a generalized formulation of a received signal strength (RSS)-based distance estimator, which was incorporated into a path loss model about the rain-induced attenuation effect, in 2018. Besides, regarding the real measurements of rain-induced impacts on mm-wave links, previous studies have demonstrated important results. Shayea *et al.* [25] demonstrated the real measurement about rain rates and rain-induced attenuation on the 26 GHz mm-wave links in 2018. Based on their results [25], a rare 120 mm/h rain rate could result in a specific rain attenuation of 26.2 dB/km. Regarding other frequency bands in mm-wave range, in 2019, Han *et al.* [26] investigated and compared the link performances under actual rain effect for three different bands (25, 28, and 38 GHz). Other studies also gave detailed discussion about rain-induced attenuations in the mm-wave bands, which were conducted worldwide corresponding to different weather conditions. In [27], Korai *et al.* discussed the impact from rain to the hybrid free space optics and radio frequency link at 28 GHz in Pakistan. Besides, Shrestha *et al.* [28] constructed a 3.2 km wireless link at 18 and 38 GHz to analyze the rain-related issue in South Korea. Mauludiyanto *et al.* [29] also analyzed a 56.4 m wireless link at 28 GHz to deal with the tropical rain attenuation in Indonesia. For higher frequency band in the mm-wave range, Hong *et al.* [30] investigated a 560 m wireless link performance at 84 GHz under real rainfalls in 2017. To further investigate the impact of rain-induced attenuation on the wireless links at THz frequency range, previous literatures also put the spotlight on it. In [31], Norouzian *et al.* compared the rain attenuation effect for mm-wave (77 GHz) and THz wave (300 GHz) under different rain rates in 2019. In addition, Hirata *et al.* [32] focused on a 400 m wireless link with V polarization at 120 GHz. Based on their work [32], the heavy rainy period data could be used for designing wireless links at THz frequency range. To provide a designing guideline for the robust wireless links towards the future beyond 5G or 6G applications worldwide, more and more researchers focused on the rain-related issue [33]–[39]. However, even these works provided comprehensive discussions about real measurement studies of rain-induced attenuations to mm-wave or THz links, none of these studies put the spotlight on the wind-induced link degradation. Since heavy wind and rain always occur together during extreme weather, it is indispensable to deal with the wind-related issue on the wireless links. In the Horizon 2020 EU–Japan project, ThoR, Jung and Kürner analyzed the performance of wireless backhaul links operating at 300 GHz [40], in which the system's performance based on ThoR hardware parameters [41] was simulated using historical weather data from the past ten years. In [42], the first concept for introducing the impact of wind was introduced. Nevertheless, to the best of our knowledge, no comprehensive evaluation of the performance degradation of the mm-wave and THz links under severe weather conditions, considering

the effects of both rain and wind, has been reported yet. This is particularly important, especially in regions where strong gust, storms, or typhoons frequently occur.

In this article, we present a comprehensive evaluation and analysis of the performance degradation of fixed wireless links under the effects of clear weather condition, rain, and wind weather conditions. The calculation of rain-induced attenuation is based on the ITU-R recommendations, which provides comprehensive parameters for the estimation. To investigate the wind effect, we propose a theoretical model, which was experimentally tested. The calculated and measured results matched well, confirming the accuracy of the proposed model for link budget evaluation. Subsequently, we analyzed the attenuations of the links under clear, rain, and wind weather conditions for the fixed wireless link at four different carrier frequencies: 75.375, 85.375, 275, and 400 GHz carriers, as the examples mentioned in the Asia-Pacific Telecommunity Wireless Group (AWG) recommendations [17]. Based on the traditional definition, extremely high-frequency (EHF) bands are between 30 and 300 GHz. In this work, 75.375, 85.375, 275 and 400 GHz carriers were analyzed and discussed. By definition, the 75.375 and 85.375 GHz carriers are sorted into millimeter wave bands and the 400 GHz carriers into THz bands. For the 275 GHz carrier, based on the ITU-R SM.2352-0 report [43], a 275 GHz carrier can be sorted into the THz band despite its wavelength being in the mm range. Hence, in this manuscript, the 75.375 and 85.375 GHz carriers are defined as mm-waves and the 275 and 400 GHz carriers as THz waves. For each link, we evaluated the signal-to-noise ratio (SNR) and maximum channel capacity under different conditions. We also estimated the maximum available transmission distance of the wireless links using a specific example of the modulation format. From the calculated results, we confirmed that attenuation by heavy rain was dominant compared to other effects. We also confirmed that the attenuation by antenna gain degradation induced by the wind effect becomes considerable for wireless links in the high-frequency band, such as at 400 GHz. The obtained results can prove useful in the design of high-reliability THz fixed wireless links that can operate under different weather conditions. The remainder of this article is organized as follows. Section II presents the attenuations, including the gaseous, rain-induced, and wind-induced attenuations. Section III presents a link budget evaluation in terms of the SNR and maximum channel capacity. Finally, Section IV concludes the article.

II. ATTENUATIONS FOR THz WIRELESS LINKS

The attenuation of the wave propagation at the THz bands considerably impacts the link performance. Under this scenario, the power attenuation of THz waves during wireless propagation is a critical issue to be investigated. In this section, the wireless attenuations due to gas (Section II-A), rain (Section II-B), and wind (Section II-C) are analyzed in detail.

A. GASEOUS ATTENUATION

THz electromagnetic waves are attenuated during wireless propagations even in a clear atmosphere. The electromagnetic waves induce oscillations of atmospheric gases (mainly oxygen) and water molecules, which results in the power degradation of the waves themselves. However, this type of attenuation cannot be removed because the atmosphere is composed of these basic molecules. Based on the ITU-R Recommendation P.676-12 [44], the overall gaseous attenuation A_{gas} (dB) can be calculated from the production of the specific gaseous attenuation γ (dB/m) and the transmission distance r_0 (m), which can be written as follows:

$$A_{gas} = \gamma r_0 = (\gamma_o + \gamma_w) \cdot r_0, \tag{1}$$

where γ is the sum of the specific attenuations due to oxygen (γ_o) and water vapor (γ_w). The specific attenuation in the atmosphere depends on the electromagnetic wave frequency. If the carrier frequency approaches the resonance frequencies of the atmospheric molecules, the gaseous attenuation increases. In addition, the magnitude reaches a relative maximum when the carrier frequency coincides with the resonance frequencies (this phenomenon can be seen in Fig. 1). The mathematical value of specific attenuation can be expressed as follows:

$$\gamma = \gamma_o + \gamma_w = 0.1820 \cdot f \cdot \left[N''_{Oxygen}(f) + N''_{WaterVapor}(f) \right], \tag{2}$$

where f is the carrier frequency (Hz). $N''_{(Oxygen)}(f)$ and $N''_{(WaterVapor)}(f)$ are the imaginary parts of the frequency-dependent complex refractivities, which can be expressed as follows:

$$N''_{Oxygen}(f) = \sum\nolimits_{i(Oxygen)} S_i F_i + N''_D(f), \tag{3}$$

$$N''_{WaterVapor}(f) = \sum\nolimits_{i(WaterVapor)} S_i F_i, \tag{4}$$

where S_i is the strength of the i^{th} oxygen or water vapor line, F_i is the line shape factor of the oxygen or water vapor, and $N''_{(D)}(f)$ is the dry continuum from pressure-induced nitrogen absorption. The aforementioned factors can be calculated using the following equations:

$$S_{i(oxygen)} = a_1 \cdot 10^{-7} \cdot p \cdot \theta^3 \cdot \exp\left[a_2 (1-\theta)\right], \tag{5}$$

$$S_{i(watervapor)} = b_1 \cdot 10^{-1} \cdot e \cdot \theta^{3.5} \cdot \exp\left[b_2 (1-\theta)\right], \tag{6}$$

$$F_i = \frac{f}{f_i} \cdot \left[\frac{\Delta f - \delta (f_i - f)}{(f_i - f)^2 + (\Delta f)^2} + \frac{\Delta f - \delta (f_i + f)}{(f_i + f)^2 + (\Delta f)^2} \right], \tag{7}$$

$$N''_D(f) = f \cdot p \cdot \theta^2 \cdot \left\{ \frac{6.14 \cdot 10^{-5}}{d \cdot \left[1 + \left(\frac{f}{d} \right)^2 \right]} + \frac{1.4 \cdot 10^{-12} \cdot p \cdot \theta^{1.5}}{1 + 1.9 \cdot 10^{-5} \cdot f^{1.5}} \right\}, \tag{8}$$

where a_i and b_i are the spectroscopic data for oxygen and water vapor attenuation, respectively, p is the dry air pressure

(hPa); e is the water vapor partial pressure (hPa), which can be calculated as $e = \rho T/216.7$ (where ρ is the water vapor density (g/m^3)), and T is the absolute temperature (K). Δf is the width of the line, δ is the correction factor, and d is the width parameter for the Debye spectrum. The other parameters can be calculated using the following equations.

$$\theta = \frac{300}{T} \tag{9}$$

$$\begin{aligned}\Delta f_{(oxygen)} &= a_3 \cdot 10^{-4} \cdot \left[p \cdot \theta^{(0.8-a_4)} + 1.1 \cdot e \cdot \theta\right] \\ &= \sqrt{(\Delta f)^2 + 2.25 \cdot 10^{-6}}\end{aligned} \tag{10}$$

$$\begin{aligned}\Delta f_{(watervapor)} &= b_3 \cdot 10^{-4} \cdot \left[p \cdot \theta^{b_4} + b_5 \cdot e \cdot \theta^{b_6}\right] \\ &= 0.535 \cdot \Delta f \\ &\quad + \sqrt{0.217 \cdot (\Delta f)^2 + \frac{2.1316 \cdot 10^{-12} \cdot f_i^2}{\theta}}\end{aligned} \tag{11}$$

$$\delta_{(oxygen)} = (a_5 + a_6 \cdot \theta) \cdot 10^{-4} \cdot (p+e) \cdot \theta^{0.8} \tag{12}$$

$$\delta_{(watervapor)} = 0 \tag{13}$$

$$d = 5.6 \cdot 10^{-4} \cdot (p+e) \cdot \theta^{0.8} \tag{14}$$

Fig. 2 illustrates the gaseous attenuation with varying transmission distance for fixed wireless links at the carrier frequencies of 75.375, 85.375, 275, and 400 GHz as calculated using (1). For the air conditions, two different cases (standard air and storm air) are included, which demonstrate different combinations of temperature, air pressure, and relative humidity. For the standard air condition, the temperature, air pressure, and relative humidity were set as 288.15 K, 1013.25 hPa, and 50.0%, respectively. However, for the storm air case, extreme weather conditions should be considered. Consequently, based on the "Tables of Climatological Normals (1991-2020)" from Japan Meteorological Agency [45], the recorded daily maximum temperature in Osaka (biggest city in western Japan) is 33.70 °C. The temperature, air pressure, and relative humidity were set as 306.85 K, 1013.25 hPa, and 100.0%, respectively. From Fig. 2, the gaseous attenuations for the mm-wave signal at 75.375 and 85.375 GHz are 0.319, and 0.306 dB, respectively, for a 1 km transmission. The attenuations increased to 1.653 dB and 2.025 dB under storm air conditions. On the other hand, the gaseous attenuation for the THz signal at 275 and 400 GHz is 3.284 and 16.636 dB for 1 km transmission because the signals are much closer to the resonance frequencies of the atmospheric molecules than the mm-wave ones. In addition, the attenuations drastically increase to 24.391 and 110.647 dB under storm air conditions, which reveals that the THz signals are more sensitive to extreme weather conditions than the mm-wave ones.

B. RAIN-INDUCED ATTENUATION

Apart from gaseous attenuation, electromagnetic waves suffer from additional attenuation during rain when propagating in free space. Because the size of the raindrops is in the range of the wavelength of THz electromagnetic waves, the

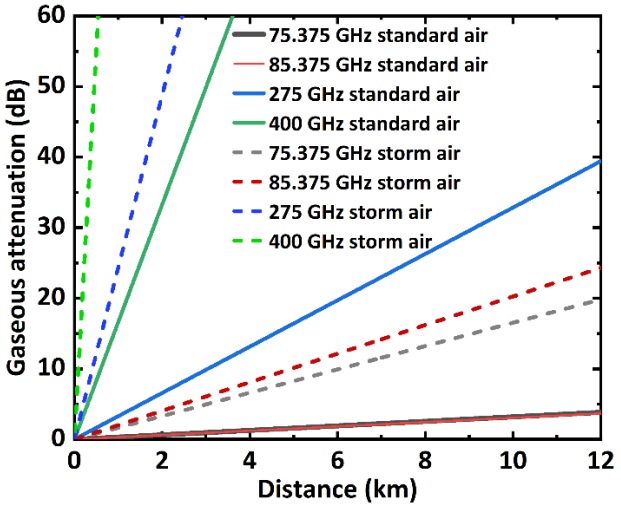

FIGURE 2. Gaseous attenuation versus transmission distance for fixed wireless links at carrier frequencies of 75.375, 85.375, 275, and 400 GHz under standard air and storm air conditions.

Mie scattering effect impacts the wireless propagation. Based on the ITU-R Recommendation P.838-3 [46], the overall rain-induced attenuation (A_{rain}) can be calculated from the production of the specific attenuation due to rain (γ_R) and the transmission distance (r_0), which can be written as follows:

$$A_{rain} = \gamma_R r_0 = k R^{\alpha} r_0, \tag{15}$$

where R is the rain rate (mm/h), k and α are either k_H and α_H (horizontal polarization) or k_V and α_V (vertical polarization), which can be calculated as follows:

$$\log_{10} k = \sum_{j=1}^{4} \left[a_j \cdot e^{-\left(\frac{\log_{10} f - b_j}{c_j}\right)^2} \right] + m_k \cdot \log_{10} f + c_k, \tag{16}$$

$$\alpha = \sum_{j=1}^{5} \left[a_j \cdot e^{-\left(\frac{\log_{10} f - b_j}{c_j}\right)^2} \right] + m_\alpha \cdot \log_{10} f + c_\alpha, \tag{17}$$

where f is the carrier frequency, and a_j, b_j, c_j, m_k, c_k, m_α, and c_α are the coefficients for calculating k_H, α_H, k_V, and α_V. Based on the tables in ITU-R Recommendation P.838-3 [46], the magnitudes of a_j, b_j, c_j, m_k, c_k, m_α, and c_α can be directly determined. Fig. 3 illustrates the rain-induced attenuation for different transmission distances for fixed wireless links at carrier frequencies of 75.375, 85.375, 275, and 400 GHz using (15).

During the calculation, the relative humidity was set to 100% and the rain rate was set to 5.4 mm/h for a moderate rain case. A 53.6 mm/h rain rate is set to represent the storm rain case as an extreme weather. In addition, 14.5 mm/h rain rate was used to represent heavy rain case [47]. In the APT-AWG-REP-81 [17], a measurement of the rain rate probability was conducted from 27th Feb. 2015 to 20th Mar. 2015. The link distance between the transmitter and receiver is approximately 2.65 km, and the channel separation is 500 MHz. The other parameters are summarized in Table 1. Besides, this

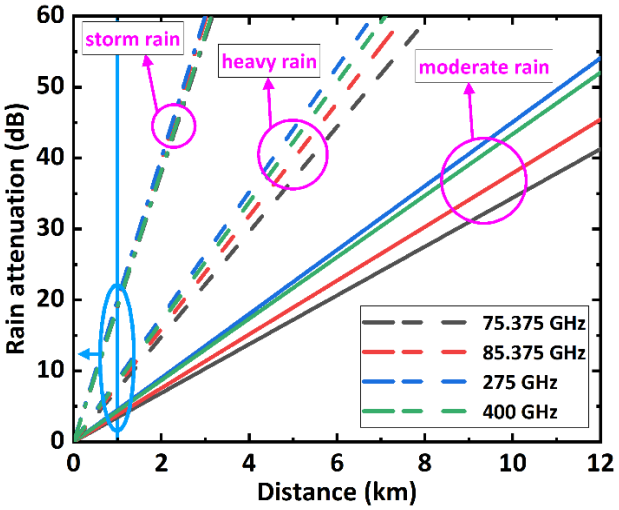

FIGURE 3. Rain-induced attenuation versus transmission distance for fixed wireless links at carrier frequencies of 75.375, 85.375, 275, and 400 GHz under different rain rates.

evaluation was conducted in an urban area in a medium-sized city in western Japan (Matsuyama City).

TABLE 1. Specifications of the radio units.

Parameter	Site A	Site B
Frequency of transmitter	75.375 GHz	85.375 GHz
Power of transmitter	+18 dBm (max) +9 dBm (min)	+18 dBm (max) +9 dBm (min)
Antenna diameter	30 cm	30 cm
Antenna gain	43 dBi	43 dBi

Based on the ITU-R Recommendation P.838-3 [46], a rain rate of 0.01% probability is a criterion for the availability calculation. Hence, we set 0.01% as the target value. According to the Ministry of Internal Affairs and Communications (MIC) Japan, the rain rate with 0.01% probability is 53.6 mm/h in Matsuyama City where the evaluation took place. In other words, 99.99% of the time has a rain rate of less than 53.6 mm/h. In addition, the value was estimated based on the cumulative distribution function of the measurement data. Consequently, it is reasonable to set 53.6 mm/h rain rate as the worst case for comparison with other cases. As indicated by the blue line in Fig. 3, the rain-induced attenuations are 3.439, 3.787, 4.507, and 4.338 dB for 75.375, 85.375, 275, and 400 GHz carriers after 1 km of propagation, respectively. The attenuations increased rapidly to 18.981, 19.818, 20.047, and 19.145 dB under a 53.6 mm/h storm rain case.

C. WIND-INDUCED ATTENUATION

The calculation model for the evaluation of the wind effect is shown in Fig. 4. We assume that the static load is applied to the pole and the antenna due to wind.

In addition, to verify the mathematical model, we set up a measurement system, as shown in Fig. 5. We observed the influence of wind on the mm-wave devices on the pole

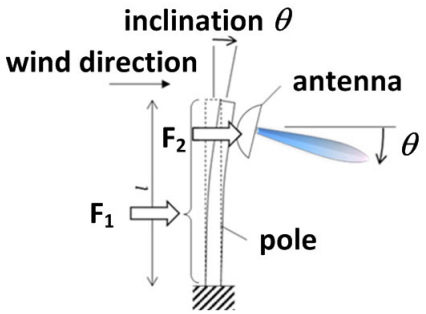

FIGURE 4. Calculation model.

for 6 months at 85.5 GHz. A parabolic antenna with a diameter of 350 mm, radio equipment, weather sensor, and acceleration sensor were installed on a steel pole with a thickness diameter of 89 mm and a length of 5 m.

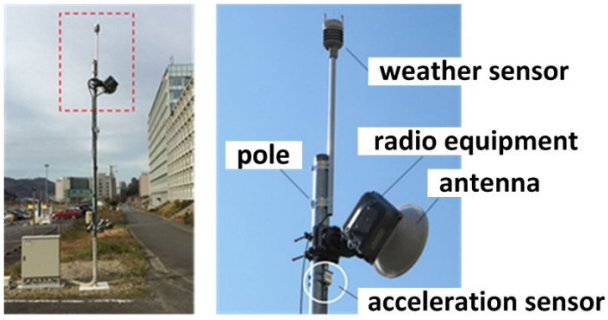

FIGURE 5. Measurement system.

In the actual systems, the antenna poles vibrate and incline when wind blows. These types of wind effects result in an inclination angle to the antenna poles, which degrades the effective gain of the antenna for fixed wireless links. To calculate the wind-induced attenuation, the estimation of the inclination angle of the antenna pole is an indispensable step. The overall inclination angle θ can be calculated as follows:

$$\theta = \theta_0 + \theta_s + \theta_d, \tag{18}$$

where θ_0 is the initial axis misalignment of the antenna pairs, θ_s is the static inclination angle, and θ_d is the dynamic inclination angle. The static and dynamic inclination angles can be calculated by:

$$\theta_s = (C_1A_1 + 3C_2A_2) \cdot \frac{\rho l^2}{12EI} v^2 \cdot \frac{180}{\pi} \equiv C_s \cdot v^2, \tag{19}$$

$$\theta_d \equiv C_d \cdot v^2, \tag{20}$$

where C_s and C_d are the wind load coefficients for static and dynamic inclination, respectively, which depend on the size and type of the antenna pole; v represents the effective wind speed; C_1 and A_1 are the drag coefficient and the wind receiving area (m^2) of the pole, respectively; C_2 and A_2 are the drag coefficient and the wind receiving area (m^2) of the antenna, respectively; ρ is the air density (kg/m^3); l is the length of the

pole (m); E is the Young's modulus (2.05×10^{11} Pa); and I is the second moment of area (m^4).

Because the wind speed is not constant, the wind speed distribution issue needs to be considered before setting a specific wind speed to calculate the inclination angle. The Weibull distribution can be employed as a model to describe the wind speed distribution as an accumulative probability function $p(v)$, which can be expressed as follows:

$$p(v) = 1-e^{-\left(\frac{v}{c}\right)^k}, \tag{21}$$

where v is the wind speed, k is the scale factor, and c is the shape factor. Based on the measurement reported in [17], the magnitude of k and c can be set to be 0.86 and 1.03, respectively. Using (21), the cumulative probability of the wind speed can be calculated as shown in Fig. 6. For consistency with the probability of rain rate calculation (Section II-B), the probability of the wind speed can also be set at 99.99% as the worst case for the storm case. As a result, the wind speed corresponding to an accumulative probability of 99.99% was 13.617 m/s, as indicated in Fig. 6. In other words, 99.99% of the time the wind speed was less than 13.617 m/s.

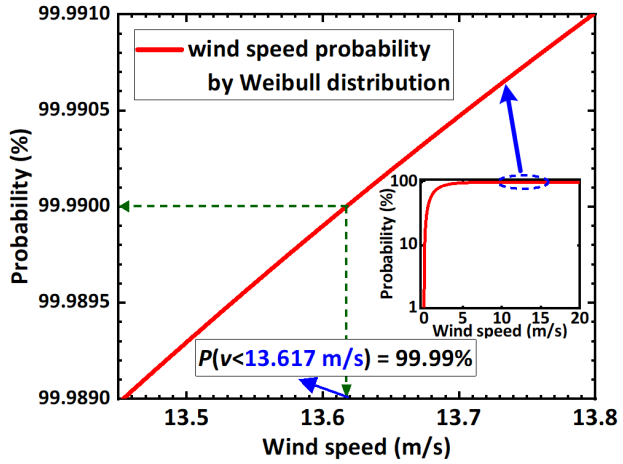

FIGURE 6. Accumulative probability distribution of wind speed by Weibull distribution model.

The static inclination angle induced by the wind effect can be estimated using (19). Table 2 summarizes an example of the parameters used to calculate the static inclination angle from the measurement system in [17]. In addition to the static inclination angle, the pole vibrates due to the wind at its natural frequency of 2.3 Hz, which results in a dynamic inclination angle. The dynamic wind load coefficient C_d under this circumstance is 4.6×10^{-4} from the measurement [17]. Using (18), (19), (20), and the parameters in Table 2, the overall inclination angle θ can be estimated as 0.142° (0.002478 rad) when the wind speed is 13.617 m/s (suppose there is no initial axis misalignment of the antenna pole pairs: $\theta_0 = 0$).

Fig. 7 shows the inclination angle calculated using the aforementioned mathematical model and the measured data from an actual measurement system [17]. For the measured

TABLE 2. Parameters for static inclination angle calculation.

Symbol	Quantity	Magnitude	Unit
C_1	drag coefficient of the pole	0.8	-
A_1	wind receiving area of the pole	0.445	m^2
C_2	drag coefficient of the antenna	1.1	-
A_2	wind receiving area of the antenna	0.0804	m^2
ρ	air density	1.226	kg/m^3
l	length of the pole	5	m
I	second moment of area	1.01×10^{-6}	m^4

data, the root-mean-square (RMS) values of the inclination angle versus wind speed were plotted. From Fig. 7, the inclination angle under a wind speed of 13.617 m/s, which corresponds to a cumulative probability distribution of 99.99%, as illustrated in Fig. 6, is 0.142°. Compared with the measurement data, the results obtained using the mathematical model were consistent. The slight difference between the measured and calculated data can be attributed to the inclusion of an initial axis alignment in the measurement system, which was not included in the calculated result.

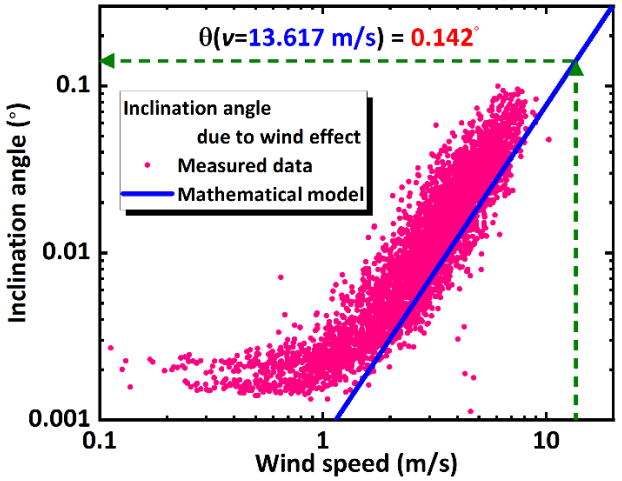

FIGURE 7. Inclination angles calculated using the mathematical model and experimental data.

The effective gain of the antennas can be estimated based on the calculated wind-induced inclination angle. The residual gain G and gain degradation due to wind-induced antenna inclination g as functions of the inclination angle θ can be calculated by

$$\mathrm{G}(\theta) = G_{\max} - g(\theta)\,(dB), \tag{22}$$

$$g(\theta) = 20\cdot\log\left[\frac{u'}{2\cdot J_1(u')}\right](dB)\left(\text{for}\frac{D}{\lambda} \le 100\right), \tag{23}$$

where G_{max} is the maximum gain of the antenna, J_1 is the Bessel function of the first kind, D is the diameter of the antenna, and λ is the wavelength of the electromagnetic waves. The other parameters can be calculated as follows:

$$u' = \frac{60\pi}{\theta_{BW}}\cdot\sin\theta, \tag{24}$$

$$\theta_{BW} = \frac{k\lambda}{D}, \tag{25}$$

where θ_{BW} is the half power beam width, and k is a factor that varies slightly depending on the shape of the reflector and the feed illumination pattern. For a typical parabolic antenna, k was approximately 70. Using the aforementioned parameters, the gain degradation and residual gain of the mm-wave carriers can be calculated. In the calculation, we assume a maximum gain G_{max} of 43 dBi, and the diameter of antenna D is assumed to be 0.3 m. The inclination angle was calculated to be 0.342° (assuming an initial axis misalignment of 0.2°). The calculated results for the 75.375 and 85.375 GHz mm-wave carriers are as follows.

$$g_{75.375GHz}(\theta = 0.342\,\text{deg}) = 1.64566\,(dB) \tag{26}$$
$$g_{85.375GHz}(\theta = 0.342\,\text{deg}) = 2.13158\,(dB) \tag{27}$$
$$G_{75.375GHz}(\theta = 0.342\,\text{deg}) = 41.35434\,(dB) \tag{28}$$
$$G_{85.375GHz}(\theta = 0.342\,\text{deg}) = 40.86842\,(dB) \tag{29}$$

From the calculated results, the gain degradations are less than 1.646 and 2.132 dB for the 75.375 and 85.375 GHz signals, respectively, in 99.99% of the time, as depicted in Figs. 6 and 7. Because of the physical constraints on the antenna diameter and signal wavelength, (23) should be employed for the mm-wave band. For the THz band, based on the ITU-R Recommendation F.699-8 [48], the residual gain can be calculated as

$$\mathrm{G}(\theta) = \max\left[\mathrm{G}_a(\theta), \mathrm{G}_b(\theta)\right](dB)\left(\text{for}\frac{D}{\lambda} > 100\right), \tag{30}$$

$$\mathrm{G}_a(\theta) = G_{\max} - 2.5\cdot 10^{-3}\cdot\left(\frac{D}{\lambda}\cdot\theta\right)^2, \tag{31}$$

$$\mathrm{G}_b(\theta) = G_1 + F(\theta), \tag{32}$$

$$G_1 = 2 + 15\cdot\log\left(\frac{D}{\lambda}\right), \tag{33}$$

$$F(\theta) = 10\cdot\log\left[0.9\cdot\sin^2\left(\frac{3\pi\theta}{2\theta_r}\right) + 0.1\right], \tag{34}$$

$$\theta_r = 15.85\cdot\left(\frac{D}{\lambda}\right)^{-0.6}(\text{deg}). \tag{35}$$

In the calculation for THz carriers, the maximum gain G_{max} and the diameter of antenna D are set to 50 dBi and 0.15 m, respectively. The other parameters remain the same for the mm-wave band. The calculated residual gains for 275 and 400 GHz carriers under the wind effect are as follows.

$$G_{275GHz}(\theta = 0.342\,\text{deg}) = 44.513\,(dB) \tag{36}$$
$$G_{400GHz}(\theta = 0.342\,\text{deg}) = 38.304\,(dB) \tag{37}$$

Compared with the original 50 dBi maximum gain, the gain degradations are 5.487 and 11.696 dB for the 275 and 400 GHz carriers, respectively, revealing that the THz band carriers are more sensitive to the wind effect than the mm-wave band.

In addition to the mentioned attenuations, the received signal power may be degraded by an additional amount owing to natural vibration, which is not included in the mathematical model. To confirm this, we compared the calculated results with the measured data. Fig. 8 shows the minimum received signal power versus the maximum wind speed for every ten seconds. The effect of each term and the approximate curve of the measurement values are also shown in the figure. According to Fig. 8, the degradation of the received signal due to misalignment of the measurement system is approximately 1.2 dB which corresponds to 0.28°. One of the factors of this difference between the two curves is that the effect of the opposite is not considered. The coefficient C_d is similar to the coefficient C_s. Both coefficients depend on the structure of the pole; therefore, a high correlation is expected, and C_d can be approximated to C_s.

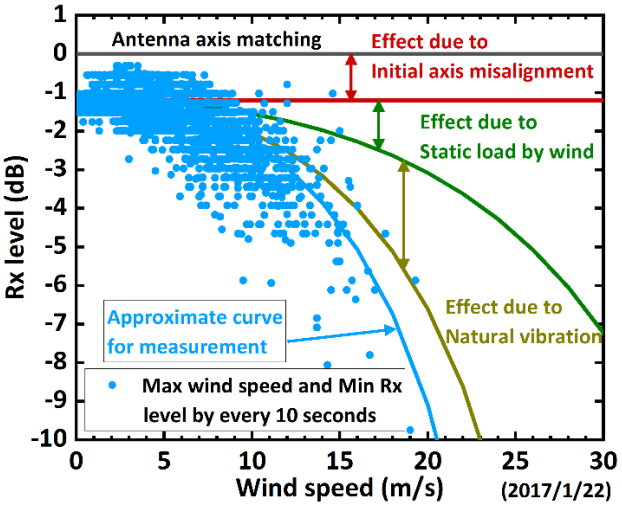

FIGURE 8. Maximum wind speed versus minimum received signal level.

III. LINK BUDGET EVALUATION

Because a fixed wireless link is regarded as an additive white Gaussian noise (AWGN) channel, the maximum achievable data rate can be defined by the maximum channel capacity C (bps/Hz), which is calculated using the Shannon formula [49] as

$$C = B\cdot\log_2(1+SNR), \tag{38}$$

where B is the signal bandwidth (Hz), and SNR is the signal-to-noise ratio of the received signal. Based on the calculations in Section II, the SNR of a fixed wireless link can be calculated as

$$SNR\,(dB) = P_{FW} + G_{FW} + G_{AP} - A_{gas} - A_{rain} - A_{wind} - A_{free} - N_{thermal} - N_{system} - M \tag{39}$$

where P_{FW} is the transmit power (dBm), G_{FW} is the gain of the transmitter antenna (dBi), G_{AP} is the gain of the receiver antenna (dBi), A_{gas} is the gaseous attenuation (dB, Section II-A), A_{rain} is the rain-induced attenuation (dB, Section II-B), A_{wind} is the wind-induced attenuation (dB, Section II-C), A_{free} is the free space loss (dB), $N_{thermal}$ is the

thermal noise power (dBm), N_{system} is the noise figure of the system, which is set to be 10 dB in our calculation, and M is an additional link margin. To calculate the free space loss, the electromagnetic wave disperses in an area that increases quadratically with the propagation distance in a wireless link. Consequently, if the effective area of the receiver antenna remains the same, the received electromagnetic wave power decreases quadratically with propagation distance. Based on the Friis formula [50], the free space loss A_{free} (dB) can be written as

$$A_{free} = 20 \cdot \log_{10}\left(\frac{4\pi f \cdot r_0}{c}\right), \tag{40}$$

where f is the carrier frequency (Hz), r_0 is the transmission distance (m), and c is the speed of light ($c = 3\times10^8$ m/s). As indicated by (40), the free space loss is frequency-dependent. In addition, when the electromagnetic wave carries a data signal, the thermal noise $N_{thermal}$ is also included in the received signal. The power of was calculated as

$$N_{thermal} = 10 \cdot \log_{10}\left(\frac{k \cdot B \cdot T}{1mW}\right), \tag{41}$$

where k is Boltzmann's constant ($k = 1.381\times10^{-23}$), B is the signal bandwidth (Hz), and T is the absolute temperature (K).

In the following calculation, an additional link margin of 5 dB was added to compensate for the gain degradation by natural vibration, as indicated in Fig. 8. The testing data bandwidth (BW) is set to 2.16 GHz as the basic BW to fit the IEEE Std. 802.15.3d-2017 [12]. In addition, a 4.32-GHz BW (two times of 2.16 GHz) testing data is also added for reference, which shows the multi-carrier transmission concept. The transmitted signal power was set to 18 dBm for all the four cases. To approach real conditions, the transmitter and receiver gains (G_{FW} and G_{AP}) for mm-wave carriers (75.375 and 85.375 GHz) are set to 43 dBi, while the transmitter and receiver gains for THz carriers (275 and 400 GHz) were set to 50 dBi. The other attenuation magnitudes are based on the results described in Section II. Table 3 summarizes the weather conditions mentioned in Fig. 9 and 10. The magnitudes of rain rate are divided into four levels: no rain, moderate rain, heavy rain, and storm rain [47]. For "storm rain" condition, the rain rate of 53.6 mm/h covers 99.99% of all cases and the temperature of 33.70°C is the recorded highest temperature in west Japan. In other words, "storm rain" can be represented as the worst case regarding the rain-induced attenuation because the remaining 0.01% only occupies nearly 8.6 s per day or 52.6 minutes per year that might not be so critical with respect to the overall system's functionality thus it can be ignored.

Case 1 (No Wind Effect): Based on (38) and (39), the expected maximum channel capacity can be estimated as shown in Fig. 9 and 10 for the cases without and with the wind effect, respectively. As shown in Fig. 9, for a basic 2.16 GHz BW case, the expected transmission distances in the ideal weather condition (without rain and wind) can extend up to more than 12 km with all four types of carrier frequencies.

TABLE 3. Parameters for each weather case [47].

Case	Rain rate	Temperature	Air pressure	Relative humidity
no rain	0.0 mm/h	15.00°C (288.15 K)	1013.25 hPa (1 atm)	50.0%
moderate rain	5.4 mm/h	15.00°C (288.15 K)	1013.25 hPa (1 atm)	100.0%
heavy rain	14.5 mm/h	33.70°C (306.85 K)	1013.25 hPa (1 atm)	100.0%
storm rain	53.6 mm/h	33.70°C (306.85 K)	1013.25 hPa (1 atm)	100.0%

However, during a 5.4 mm/h moderate rain without wind, the expected transmission distances for 2.16 GHz BW degraded to approximately 6 km owing to the Mie scattering effect. Furthermore, in an extreme 53.6 mm/h rain rate, no more than 2 km transmission distance is allowed for these four types of carrier frequencies even without wind effect. In addition, either the basic 2.16 GHz BW or the 4.32 GHz BW exhibit a similar trend in this condition.

Case 2 (Wind Effect on Transmitter and Receiver Antennas): Compared with the aforementioned results, in this subsection, not only rain and gaseous attenuation (clear atmosphere), but wind-induced degradation is considered. As described in section II-C, the wind speed of 13.617 m/s is the worst case within 99.99% of all situations. Consequently, the 53.6 mm/h rain rate with wind effect can be regarded as an extreme weather condition (storm), and the calculated maximum channel capacities can be regarded as the least achievable performance of the corresponding fixed wireless link. As shown in Fig. 10, for mm-wave carriers (75.375 and 85.375 GHz) with extreme wind effects, the expected transmission distances are almost the same as those without the wind effect because the maximum gain degradation for a single antenna is only approximately 2.1 dB. On the other hand, for THz carriers (275 and 400 GHz), the expected transmission distances deteriorate sharply with extreme wind effects. This stems from the antenna's radiation pattern, whose main lobe becomes narrower and steeper as the transmission frequency increases. Comparing Fig. 10(c) with Fig. 9(c), for the 275 GHz carrier, although 12-km transmission distance can be expected without rain regardless of the wind effect, the maximum transmission distance decreases from approximately 6 km to approximately 4 km under the impact of extreme wind. Moreover, the magnitude further shortens to less than 2 km with 53.6 mm/h rain rate. In particular, approximately up to 23.392 dB degradation due to wind is suffered by a 400 GHz fixed wireless link using a 50 dBi gain antenna in the extreme case. From Fig. 10(d), the maximum transmission distance for the 400 GHz carrier is only approximately 6 km under extreme wind effects, even without rain. In addition, the 4.32 GHz BW can only be transmitted at approximately 4 km because of the lack of SNR with extreme wind effects even without rain. Consequently, the THz wireless link must be precisely designed in regions with frequent extreme weather conditions.

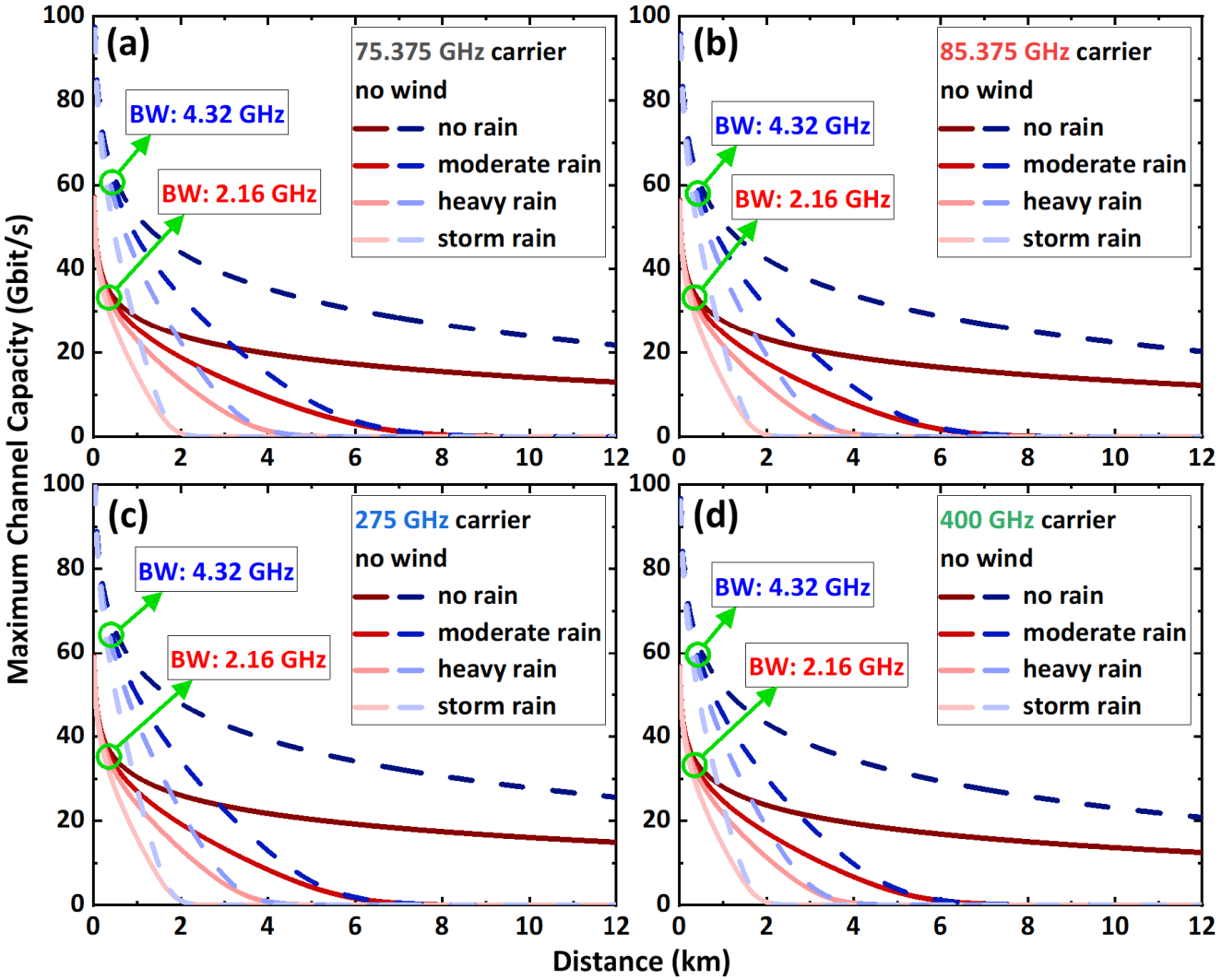

FIGURE 9. Estimated maximum channel capacity versus transmission distance using 2.16 and 4.32 GHz bandwidth for a fixed wireless link at carrier frequency of: (a) 75.375 GHz, (b) 85.375 GHz, (c) 275 GHz, and (d) 400 GHz (without wind effect).

Based on the aforementioned results, the expected maximum channel capacities for each frequency carrier under different weather conditions can be further discussed. Fig. 11 illustrates the maximum channel capacity versus transmission distance for a fixed wireless link at the carrier frequencies of (a) 75.375 GHz, (b) 85.375 GHz, (c) 275 GHz, and (d) 400 GHz under different weather conditions. The signal BW used in the calculation is 2.16 GHz as an example for the IEEE Std. 802.15.3d-2017 [12]. The data shown in Fig. 11 were extracted from Fig. 9 and 10. The weather conditions shown in Fig. 11 are listed in Table 4.

From Fig. 11, the pure wind-induced maximum channel capacity deteriorations are much less than those of pure rain-induced ones for 75.375, 85.375, and 275 GHz carriers. In other words, the rain effect dominates the fixed wireless link deterioration in these frequency ranges. On the other hand, the maximum transmission distance for the 400 GHz carrier under the wind effect is approximately the same as that under 5.4 mm/h rain effect (moderate rain). In other words, the rain effect no longer dominates the link deterioration, and the impact of wind should be considered for a 400 GHz carrier-based fixed wireless link.

As shown in Fig. 11, the transmission distances for the four carriers can be longer than 12 km under ideal weather conditions (without wind or rain effects). In contrast, the

TABLE 4. Weather conditions for maximum channel capacity calculation.

Case	Rain rate (mm/h)	Wind speed (m/s)
ideal	0.0	0.000
moderate rain only	5.4	0.000
heavy rain only	14.5	0.000
storm rain only	53.6	0.000
wind only	0.0	13.617
storm	53.6	13.617

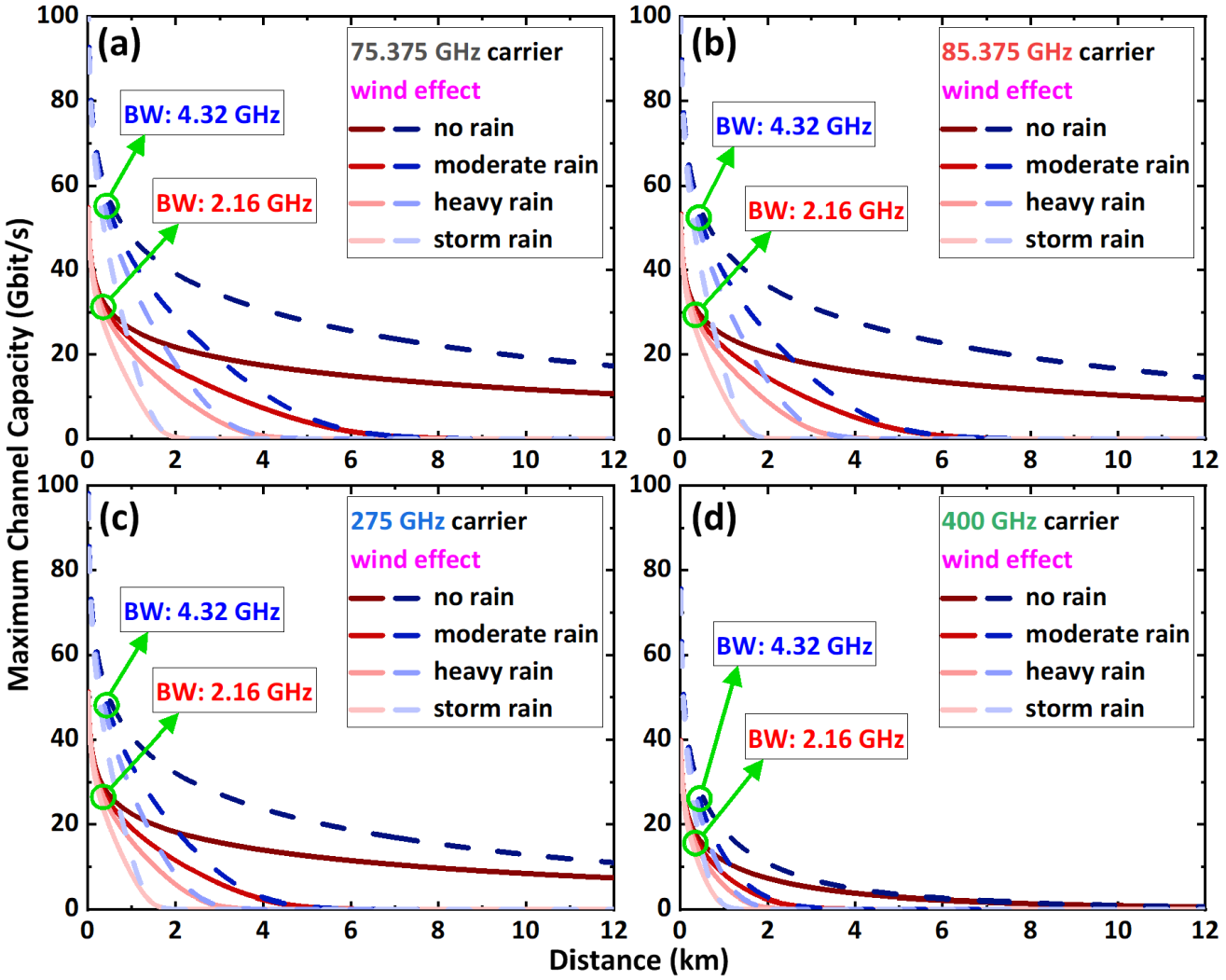

FIGURE 10. Estimated maximum channel capacity versus transmission distance using 2.16 and 4.32 GHz bandwidth for a fixed wireless link at carrier frequency of: (a) 75.375 GHz, (b) 85.375 GHz, (c) 275 GHz, and (d) 400 GHz (with wind effect).

transmission distances in the storm case (with 13.617 m/s wind and 51.6 mm/h rain) shrink significantly to less than 2 km. We further discuss the system under severe weather conditions as follows: Fig. 12 illustrates the calculated SNRs versus transmission distance for different carrier frequencies in the storm case for a fixed wireless link based on (39). The signal BW is 2.16 GHz.

To evaluate the maximum available transmission distance in a practical system, we use the bit error rate (BER) relation for the M-ary phase-shift keying (M-PSK) signal as follows [51]:

$$BER_{M-PSK} \cong \frac{2}{\max\left[\log_2(M), 2\right]} \cdot \sum_{i=1}^{\max\left(\frac{M}{4}, 1\right)} Q\left\{\sqrt{2 \cdot SNR} \cdot \sin\left[\frac{(2i-1)\pi}{M}\right]\right\} \tag{42}$$

where M is for M-PSK data, and Q is the Q-function, which can be expressed as

$$Q(x) = \frac{1}{\sqrt{2\pi}} \int_x^{\infty} e^{-\frac{t^2}{2}} dt = \frac{1}{2} erfc\left(\frac{x}{\sqrt{2}}\right), \tag{43}$$

where *erfc* is the complementary error function as

$$erfc(x) = \frac{2}{\sqrt{\pi}} \int_x^{\infty} e^{-t^2} dt. \tag{44}$$

For binary phase shift keying (BPSK), $M = 2$, the BER calculation can be simplified as follows.

$$BER_{BPSK} \cong Q\left(\sqrt{2 \cdot SNR}\right) = \frac{1}{2} \cdot erfc\left(\sqrt{SNR}\right) \tag{45}$$

In addition, if the employed data format is higher modulation constellation scheme like quadrature phase-shift keying (QPSK), 16-quadrature amplitude modulation

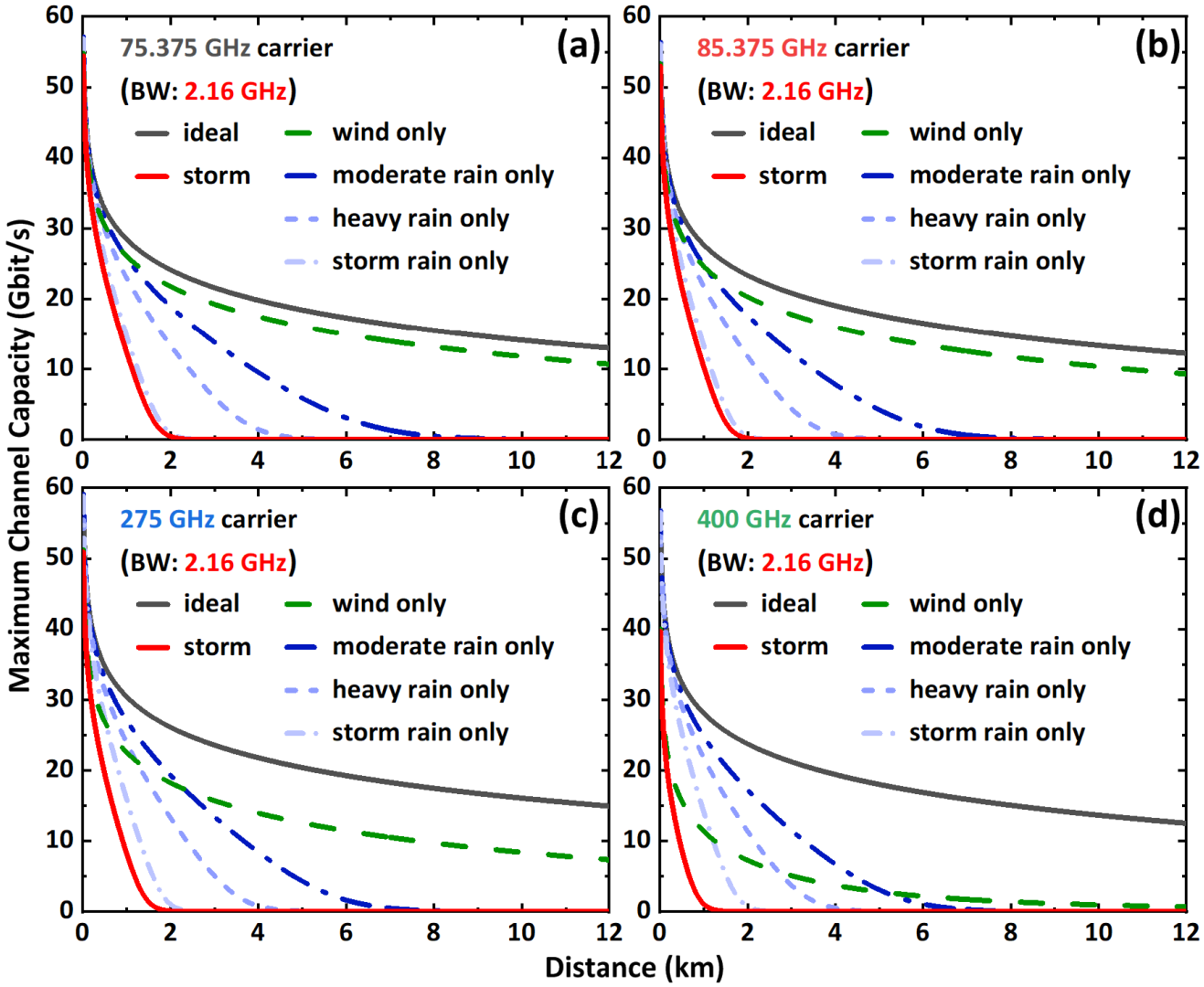

FIGURE 11. Estimated maximum channel capacity versus transmission distance for a fixed wireless link with carrier frequency of (a) 75.375 GHz, (b) 85.375 GHz, (c) 275 GHz, and (d) 400 GHz under different kinds of weather conditions.

(16-QAM), or 64-QAM, the BER relations with SNR are as follows [52].

$$BER_{QPSK} \cong \frac{1}{2}\cdot erfc\left(\sqrt{\frac{1}{2}\cdot SNR}\right) \quad (46)$$

$$BER_{16-QAM} \cong \frac{3}{8}\cdot erfc\left(\sqrt{\frac{1}{10}\cdot SNR}\right) \quad (47)$$

$$BER_{64-QAM} \cong \frac{7}{24}\cdot erfc\left(\sqrt{\frac{1}{42}\cdot SNR}\right) \quad (48)$$

Fig. 13 shows the calculated BERs in the storm case for a fixed wireless link based on (46), (47), and (48) with the results in Fig. 12. The BER threshold of 3.8×10^{-3} considering a 7% forward error correction (FEC) overhead [53], is also shown in the figure.

From Fig. 13, the maximum available transmission distances for a 2.16 GHz BPSK, QPSK, 16-QAM, and 64-QAM data with different carrier frequencies in the storm case can be estimated by taking the x-axis magnitudes from the intersections of the FEC criterion dotted

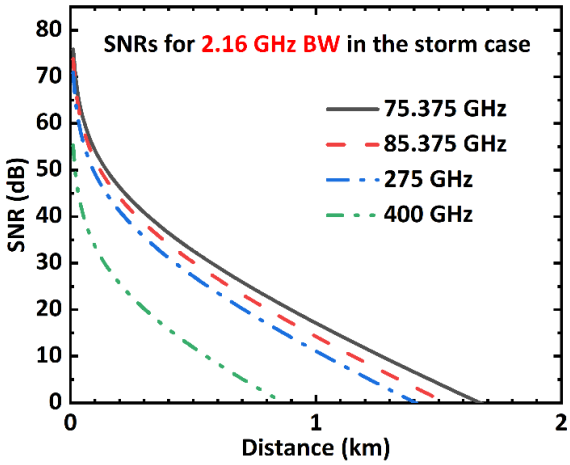

FIGURE 12. Calculated SNRs versus transmission distance in the storm case for a fixed wireless link at carrier frequency of 75.375 GHz, 85.375 GHz, 275 GHz, and 400 GHz.

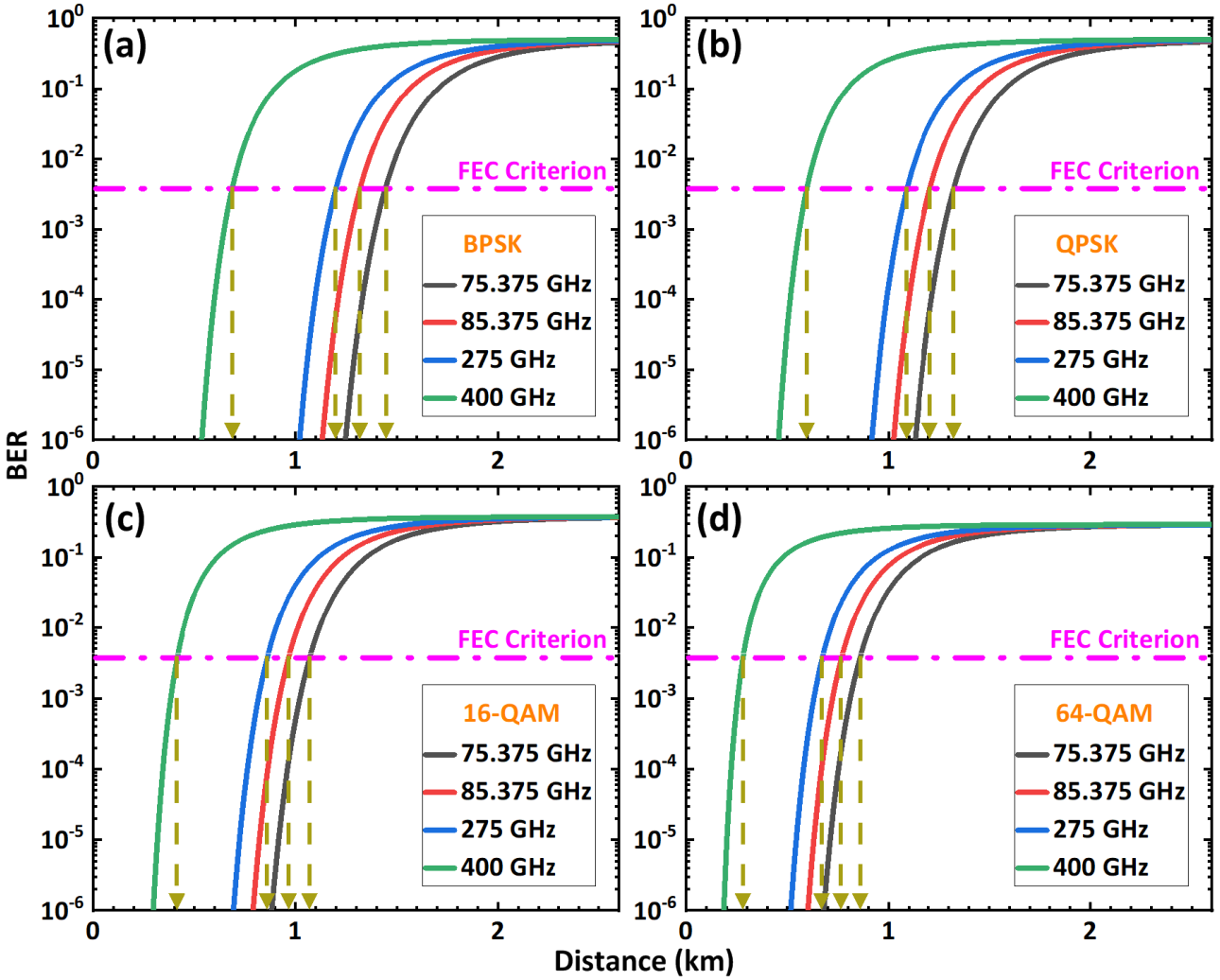

FIGURE 13. Calculated BERs of (a) BPSK, (b) QPSK, (c) 16-QAM, and (d) 64-QAM data formats versus transmission distance in the storm case for a fixed wireless link at carrier frequencies of 75.375, 85.375, 275, and 400 GHz.

TABLE 5. Maximum available transmission distances in storm case.

Carrier frequency	BPSK	QPSK	16-QAM	64-QAM
75.375 GHz	1443 m	1324 m	1071 m	859 m
85.375 GHz	1317 m	1206 m	968 m	768 m
275 GHz	1199 m	1091 m	862 m	672 m
400 GHz	688 m	596 m	414 m	281 m

line and the BER curves, which are summarized in Table 5.

Based on Table 5, when adopting BPSK or QPSK as the data format, all the maximum available transmission distances exceeded 1 km for 75.375, 85.375, and 275 GHz carriers under storm conditions. However, for the 400 GHz system, the maximum available transmission distances reduce sharply to 688 m (BPSK) and 596 m (QPSK) owing to the significant reduction in the SNR. On the other hand, when adopting a much higher modulation constellation scheme (e.g., 16-QAM or 64-QAM), the expected maximum available transmission distances hardly exceed 1 km because the required SNRs of these schemes are higher than those of BPSK and QPSK. As described above, the 400 GHz carrier is very sensitive to wind and rain effects; thus, the fixed wireless link using radio signals in this frequency band should be limited to a few hundreds of meters.

In practical systems, the wind speed effect due to pole vibration depends on the pole shape, dimensions, manufacturing material, position, and type of fixing on the ground. By strictly fixing the pole to the ground or fixing the antenna on a wall or tower, the pole vibration induced wind effect can be minimized. However, even the trivial vibration cannot be totally ignored [54], [55]. Recently, solutions for the beam direction fluctuation have been raised for a mm-wave fixed wireless system. For example, the automatic transmit power control (ATPC) technology is supposed to deal with

such an issue [17]. With ATPC, the transmitter's power can be automatically controlled by the detector at receiver side, which suppresses the fluctuation range of the received signal level to be smaller than the fluctuation range of the channel attenuation. Furthermore, for the future beyond 5G or 6G applications, constructing a ubiquitous wireless link is indispensable. In this circumstance, since the attenuation for THz waves are high even without any interference in free space, the number of base stations for beyond 5G or 6G links should be enough to ensure the coverage of all the client areas [56]–[58]. However, it is difficult to build robust base stations like radio towers everywhere due to constructing cost or space issues. Hence, cost-effective base stations with minimized sizes are the targets for beyond 5G or 6G links. In these cases, it is necessary to consider the pole vibration effect into link budget evaluation. The proposed antenna pole structure in this manuscript can demonstrate a good example for future usage in beyond 5G or 6G networks. Nevertheless, a comprehensive evaluation on the effect of pole vibration considering different pole shapes, dimensions, manufacturing materials, positions, and types of fixing on the ground is essential to evaluate the fixed wireless link performance under extreme weather conditions and should be investigated in the future works.

IV. CONCLUSION

This article presents a comprehensive discussion of fixed wireless links in the mm-wave and THz bands under extreme weather conditions. The characteristics at four carrier frequencies, 75.375, 85.375, 275, and 400 GHz, are discussed in detail. Link budget evaluations for each carrier frequency were also conducted. For gaseous attenuation, mm-wave carriers barely suffer from air-induced attenuation within 12 km. On the other hand, THz waves exhibit severe gaseous attenuation even in standard air. For the storm case, the attenuation rates for all four types of carrier frequencies increase, which means that either mm-waves or THz waves are sensitive to humidity and temperature. Next, during the analysis of rain attenuation, the rain rate dominated the overall rain-induced attenuation regardless of the frequency of different carriers. In addition, the rain rate of 53.6 mm/h can be reasonably regarded as the worst case for further calculations. For the wind-related calculations, two different models are employed, and a wind speed of 13.617 m/s can be regarded as the worst case (99.99%). A 2.16 GHz data is employed for the maximum channel capacity evaluations. During the analysis, only the 400 GHz carrier was relatively sensitive to severe wind effects. In addition, the rain effect dominates the deterioration of the link performance regardless of the carrier frequency. Finally, the maximum available transmission distances of 2.16 GHz BPSK, QPSK, 16-QAM, and 64-QAM data for each frequency carrier under extreme weather (storm) were obtained, providing input to the planning process of wireless backhaul/fronthaul links at mm-wave and THz frequencies.

APPENDIX

TABLE 6. Abbreviation list.

Abbreviation	Meaning
5G	5th generation
6G	6th generation
APT	Asia-Pacific Telecommunity
ATPC	automatic transmit power control
AWG	Asia-Pacific Telecommunity Wireless Group
AWGN	additive white Gaussian noise
BER	bit error rate
BPSK	binary phase shift keying
BW	bandwidth
COVID-19	coronavirus disease 2019
EHF	extremely high-frequency
FEC	forward error correction
IEEE	Institute of Electrical and Electronics Engineers
ITU	International Telecommunication Union
ITU-R	ITU Radiocommunication Sector
M-PSK	M-ary phase-shift keying
mm-wave	millimeter-wave
MIC	Ministry of Internal Affairs and Communications
QAM	quadrature amplitude modulation
QPSK	quadrature phase shift keying
REP	report
RMS	root-mean-square
RSS	received signal strength
SNR	signal-to-noise ratio
Std.	standard
THz	terahertz
WRC-19	World Radiocommunication Conference 2019

ACKNOWLEDGMENT

The THz-wave transmission study presented in Section II was performed as a part of ThoR (TeraHertz end-to-end wireless systems supporting ultra-high data Rate applications) project funded in part by the Horizon 2020, the European Union's Framework Programme for Research and Innovation, under Agreement 814523, and in part by the Commissioned Research (No. 196) of the National Institute of Information and Communications Technology (NICT), Japan. The 400 GHz transmission study was partly conducted under the contract "R&D of high-speed THz communication based on radio and optical direct conversion" by the Ministry of Internal Affairs and Communications of Japan under Grant JPJ000254. The millimeter-wave transmission analysis under heavy rain and 275 GHz THz link study were obtained from the commissioned research: No.00401 and No.00302, funded by NICT.

REFERENCES

[1] M. Agiwal, A. Roy, and N. Saxena, "Next generation 5G wireless networks: A comprehensive survey," *IEEE Commun. Surveys Tuts.*, vol. 18, no. 3, pp. 1617–1655, 3rd Quart., 2016.
[2] E. Dahlman, G. Mildh, S. Parkvall, J. Peisa, J. Sachs, Y. Selén, and J. Sköld, "5G wireless access: Requirements and realization," *IEEE Commun. Mag.*, vol. 52, no. 12, pp. 42–47, Dec. 2014.
[3] S. Hossain, "5G wireless communication systems," *Amer. J. Eng. Res.*, vol. 2, no. 10, pp. 344–353, 2013.
[4] M. A. M. Albreem, "5G wireless communication systems: Vision and challenges," in *Proc. Int. Conf. Comput., Commun., Control Technol. (I4CT)*, Apr. 2015, pp. 493–497.

[5] W. Saad, M. Bennis, and M. Chen, "A vision of 6G wireless systems: Applications, trends, technologies, and open research problems," *IEEE Netw.*, vol. 34, no. 3, pp. 134–142, May/Jun. 2020.

[6] Z. Zhang, Y. Xiao, Z. Ma, M. Xiao, Z. Ding, X. Lei, G. K. Karagiannidis, and P. Fan, "6G wireless networks: Vision, requirements, architecture, and key technologies," *IEEE Veh. Technol. Mag.*, vol. 14, no. 3, pp. 28–41, Sep. 2019.

[7] K. B. Letaief, W. Chen, Y. Shi, J. Zhang, and Y.-J.-A. Zhang, "The roadmap to 6G: AI empowered wireless networks," *IEEE Commun. Mag.*, vol. 57, no. 8, pp. 84–90, Aug. 2019.

[8] P. Yang, Y. Xiao, M. Xiao, and S. Li, "6G Wireless communications: Vision and potential techniques," *IEEE Netw.*, vol. 33, no. 4, pp. 70–75, Jul./Aug. 2019.

[9] T. S. Rappaport, Y. Xing, O. Kanhere, S. Ju, A. Madanayake, S. Mandal, A. Alkhateeb, and G. C. Trichopoulos, "Wireless communications and applications above 100 GHz: Opportunities and challenges for 6G and beyond," *IEEE Access*, vol. 7, pp. 78729–78757, 2019.

[10] H. Tataria, M. Shafi, A. F. Molisch, M. Dohler, H. Sjoland, and F. Tufvesson, "6G wireless systems: Vision, requirements, challenges, insights, and opportunities," *Proc. IEEE*, vol. 109, no. 7, pp. 1166–1199, Jul. 2021.

[11] C. Chaccour, M. N. Soorki, W. Saad, M. Bennis, P. Popovski, and M. Debbah, "Seven defining features of terahertz (THz) wireless systems: A fellowship of communication and sensing," 2021, *arXiv:2102.07668*.

[12] V. Petrov, T. Kurner, and I. Hosako, "IEEE 802.15.3d: First standardization efforts for sub-terahertz band communications toward 6G," *IEEE Commun. Mag.*, vol. 58, no. 11, pp. 28–33, Nov. 2020.

[13] B. K. Jung, N. Dreyer, J. M. Eckhard, and T. Kurner, "Simulation and automatic planning of 300 GHz backhaul links," in *Proc. 44th Int. Conf. Infr., Millim., THz Waves (IRMMW-THz)*, Sep. 2019, pp. 1–3, doi: 10.1109/IRMMW-THz.2019.8873734.

[14] B. K. Jung and T. Kurner, "Automatic planning algorithm of 300 GHz backhaul links using ring topology," in *Proc. 15th Eur. Conf. Antennas Propag. (EuCAP)*, Mar. 2021, pp. 1–5, doi: 10.23919/EuCAP51087.2021.9411010.

[15] R. Okumura and A. Hirata, "Automatic planning of 300-GHz-band wireless backhaul link deployment in metropolitan area," in *Proc. Int. Symp. Antennas Propag. (ISAP)*, Jan. 2021, pp. 541–542, doi: 10.23919/ISAP47053.2021.9391385.

[16] T. Kurner and B. K. Jung, "Automatic planning of NLOS backhaul links at 300 GHz arranged in star topology," in *Proc. Gen. Assem. Sci. Symp. Int. Union Radio Sci. (URSI GASS)*, Aug. 2021, pp. 1–4.

[17] (Apr. 2018). *APT-AWG-REP-81, APT Report on FWS Link Performance Under Severe Weather Conditions*. [Online]. Available: https://www.apt.int/AWG-REPTS

[18] *WRC-19 Final Acts*, ITU Publications, Geneva, Switzerland, Mar. 2020, pp. 1–666.

[19] T. Kurner and A. Hirata, "On the impact of the results of WRC 2019 on THz communications," in *Proc. 3rd Int. Workshop Mobile THz Syst. (IWMTS)*, Jul. 2020, pp. 1–3, doi: 10.1109/IWMTS49292.2020.9166206.

[20] I. A. Hemadeh, K. Satyanarayana, M. El-Hajjar, and L. Hanzo, "Millimeter-wave communications: Physical channel models, design considerations, antenna constructions, and link-budget," *IEEE Commun. Surveys Tuts.*, vol. 20, no. 2, pp. 870–913, 2nd Quart., 2018.

[21] M. E. Leinonen, G. Destino, O. Kursu, M. Sonkki, and A. Pärssinen, "28 GHz wireless backhaul transceiver characterization and radio link budget," *ETRI J.*, vol. 40, no. 1, pp. 89–100, 2018.

[22] K. Rikkinen, P. Kyosti, M. E. Leinonen, M. Berg, and A. Parssinen, "THz radio communication: Link budget analysis toward 6G," *IEEE Commun. Mag.*, vol. 58, no. 11, pp. 22–27, Nov. 2020.

[23] T. Schneider, A. Wiatrek, S. Preußler, M. Grigat, and R.-P. Braun, "Link budget analysis for terahertz fixed wireless links," *IEEE Trans. THz Sci. Technol.*, vol. 2, no. 2, pp. 250–256, Mar. 2012.

[24] S.-H. Fang, Y.-C. Cheng, and Y.-R. Chien, "Exploiting sensed radio strength and precipitation for improved distance estimation," *IEEE Sensors J.*, vol. 18, no. 16, pp. 6863–6873, Aug. 2018.

[25] I. Shayea, T. A. Rahman, M. H. Azmi, and M. R. Islam, "Real measurement study for rain rate and rain attenuation conducted over 26 GHz microwave 5G link system in Malaysia," *IEEE Access*, vol. 6, pp. 19044–19064, 2018.

[26] C. Han, Y. Bi, S. Duan, and G. Lu, "Rain rate retrieval test from 25-GHz, 28-GHz, and 38-GHz millimeter-wave link measurement in Beijing," *IEEE J. Sel. Topics Appl. Earth Observ. Remote Sens.*, vol. 12, no. 8, pp. 2835–2847, Aug. 2019.

[27] U. A. Korai, L. Luini, R. Nebuloni, and I. Glesk, "Statistics of attenuation due to rain affecting hybrid FSO/RF link: Application for 5G networks," in *Proc. 11th Eur. Conf. Antennas Propag. (EUCAP)*, Mar. 2017, pp. 1789–1792.

[28] S. Shrestha and D.-Y. Choi, "Rain attenuation over terrestrial microwave links in South Korea," *IET Microw., Antennas Propag.*, vol. 11, no. 7, pp. 1031–1039, Jun. 2017.

[29] A. Mauludiyanto, G. Hendrantoro, M. H. Purnomo, T. Ramadhany, and A. Matsushima, "ARIMA modeling of tropical rain attenuation on a short 28-GHz terrestrial link," *IEEE Antennas Wireless Propag. Lett.*, vol. 9, pp. 223–227, 2010.

[30] E. Hong, S. Lane, D. Murrell, N. Tarasenko, and C. Christodoulou, "Terrestrial link rain attenuation measurements at 84 GHz," in *Proc. United States Nat. Committee URSI Nat. Radio Sci. Meeting (USNC-URSI NRSM)*, Jan. 2017, pp. 1–2.

[31] F. Norouzian, E. Marchetti, M. Gashinova, E. Hoare, C. Constantinou, P. Gardner, and M. Cherniakov, "Rain attenuation at millimeter wave and low-THz frequencies," *IEEE Trans. Antennas Propag.*, vol. 68, no. 1, pp. 421–431, Jan. 2020.

[32] A. Hirata, R. Yamaguchi, H. Takahashi, T. Kosugi, K. Murata, N. Kukutsu, and Y. Kado, "Effect of rain attenuation for a 10-Gb/s 120-GHz-band millimeter-wave wireless link," *IEEE Trans. Microw. Theory Techn.*, vol. 57, no. 12, pp. 3099–3105, Dec. 2009.

[33] A. A. H. Budalal, M. R. Islam, K. Abdullah, and T. A. Rahman, "Modification of distance factor in rain attenuation prediction for short-range millimeter-wave links," *IEEE Antennas Wireless Propag. Lett.*, vol. 19, no. 6, pp. 1027–1031, Jun. 2020.

[34] Z. Qingling and J. Li, "Rain attenuation in millimeter wave ranges," in *Proc. 7th Int. Symp. Antennas, Propag. EM Theory*, Oct. 2006, pp. 1–4.

[35] G. O. Ajayi and E. B. C. Ofoche, "Some tropical rainfall rate characteristics at Ile–Ife for microwave and millimeter wave applications," *J. Climate Appl. Meteorol.*, vol. 23, no. 4, pp. 562–567, Apr. 1984.

[36] J. Huang, Y. Cao, X. Raimundo, A. Cheema, and S. Salous, "Rain statistics investigation and rain attenuation modeling for millimeter wave short-range fixed links," *IEEE Access*, vol. 7, pp. 156110–156120, 2019.

[37] T. Utsunomiya and M. Sekine, "Rain attenuation at 103 GHz in millimeter wave ranges," *Int. J. Infr. Millim. Waves*, vol. 26, no. 11, pp. 1651–1660, Nov. 2005.

[38] E. S. Hong, S. Lane, D. Murrell, N. Tarasenko, C. Christodoulou, and J. Keeley, "Estimating rain attenuation at 72 and 84 GHz from raindrop size distribution measurements in Albuquerque, NM, USA," *IEEE Geosci. Remote Sens. Lett.*, vol. 16, no. 8, pp. 1175–1179, Aug. 2019.

[39] A. M. Al-Samman, M. Mohamed, Y. Ai, M. Cheffena, M. H. Azmi, and T. A. Rahman, "Rain attenuation measurements and analysis at 73 GHz E-band link in tropical region," *IEEE Commun. Lett.*, vol. 24, no. 7, pp. 1368–1372, Jul. 2020.

[40] B. K. Jung and T. Kürner, "Performance analysis of 300 GHz backhaul links using historic weather data," *Adv. Radio Sci.*, to be published.

[41] (2018). *ThoR D5.2, Preliminary Antenna, Propagation and Channel Models*. [Online]. Available: https://thorproject.eu/wp-content/uploads/2021/02/ThoR-D5.2-Preliminary-antenna-propagation-and-channel-models.pdf

[42] T. Kurner, A. Hirata, B. K. Jung, E. Sasaki, P. Jurcik, and T. Kawanishi, "Towards propagation and channel models for the simulation and planning of 300 GHz backhaul/fronthaul links," in *Proc. XXXIII Gen. Assem. Sci. Symp. Int. Union Radio Sci.*, Aug. 2020, pp. 1–4, doi: 10.23919/URSI-GASS49373.2020.9232186.

[43] *Technology Trends of Active Services in the Frequency Range 275–3000 GHz*, document ITU-R SM.2352-0, ITU, 2015.

[44] *Attenuation by Atmospheric Gases and Related Effects*, document ITU-R P.676-12, ITU, 2019.

[45] Japan Meteorological Agency. *Tables of Climatological Normals (1991–2020)*. Accessed: Nov. 8, 2021. [Online]. Available: https://www.data.jma.go.jp/obd/stats/data/en/normal/normal.html

[46] *Specific Attenuation Model for Rain for Use in Prediction Methods*, document ITU-R P.838-3, ITU, 2005.

[47] Met Office, Exeter, U.K. *Fact Sheet No. 3—Water in the Atmosphere, National Meteorological Library and Archive*. [Online]. Available: https://web.archive.org/web/20120114162401/http://www.metoffice.gov.U.K./media/pdf/4/1/No._03_-_Water_in_the_Atmosphere.pdf

[48] *Reference Radiation Patterns for Fixed Wireless System Antennas for Use in Coordination Studies and Interference Assessment in the Frequency Range From 100 MHz to 86 GHz*, document ITU-R F.699-8, ITU, 2018.

[49] C. E. Shannon, "Communication in the presence of noise," *Proc. IRE*, vol. 37, no. 1, pp. 10–21, 1949.
[50] H. T. Friis, "A note on a simple transmission formula," *Proc. IRE*, vol. 34, no. 5, pp. 254–256, 1946.
[51] J. Lu, K. B. Letaief, J. C.-I. Chuang, and M. L. Liou, "M-PSK and M-QAM BER computation using signal-space concepts," *IEEE Trans. Commun.*, vol. 47, no. 2, pp. 181–184, Feb. 1999.
[52] J. G. Proakis, *Digital Communications*. New York, NY, USA: McGraw-Hill, 2001, pp. 777–778.
[53] *Forward Error Correction for High Bit-Rate DWDM Submarine Systems*, document ITU-T G.975.1, ITU, 2004.
[54] *Environmental Engineering (EE); Analysis of Test Method and Test Severity for Mechanical Test of Equipment Installed on Poles/Towers*, Standard ETSI TR 103 538, Version 1.1.1, 2019. [Online]. Available: https://www.etsi.org/deliver/etsi_tr/103500_103599/103538/01.01.01_60/tr_103538v010101p.pdf
[55] J. Otero, P. Yalamanchili, and H.-W. Braun. (2001). *High Performance Wireless Networking and Weather, High Performance Wireless Research and Education Network*. [Online]. Available: http://hpwren.ucsd.edu/info/images/weather.pdf
[56] T. Kawanishi, "THz and photonic seamless communications," *J. Lightw. Technol.*, vol. 37, no. 7, pp. 1671–1679, Apr. 1, 2019.
[57] J. Saunders and N. Marshall. (2018). Mobile backhaul options-spectrum analysis and recommendations. GSM Association. [Online]. Available: https://www.gsma.com/spectrum/wp-content/uploads/2019/04/Mobile-Backhaul-Options.pdf
[58] T. Kawanishi, A. Kanno, and H. S. C. Freire, "Wired and wireless links to bridge networks: Seamlessly connecting radio and optical technologies for 5G networks," *IEEE Microw. Mag.*, vol. 19, no. 3, pp. 102–111, May 2018.

ZU-KAI WENG received the B.S. degree from the Department of Engineering Science and Ocean Engineering, National Taiwan University, Taipei, Taiwan, in 2015, and the M.S. degree from the Graduate Institute of Photonics and Optoelectronics, National Taiwan University, Taipei, in 2017. He is currently pursuing the Ph.D. degree with the Department of Electronic and Physical Systems, Graduate School of Fundamental Science and Engineering, Waseda University, Tokyo, Japan. His research focuses on injection-locked semiconductor lasers, fiber-optic communication systems, long-reach dense wavelength division multiplexing passive optical networks, all-optical millimeter-wave generation, digital radio-over-fiber constructions, delta-sigma modulation, millimeter-waves, THz fixed wireless links, orthogonal frequency division multiplexing, and universal filtered multicarrier.

ATSUSHI KANNO (Member, IEEE) received the B.Sci., M.Sci., and Ph.D. degrees in science from the University of Tsukuba, Japan, in 1999, 2001, and 2005, respectively. In 2005, he was with the Venture Business Laboratory, Institute of Science and Engineering, University of Tsukuba. In 2006, he joined the National Institute of Information and Communications Technology (NICT), Japan, where he is currently the Director of the Optical Access Technology Laboratory, Photonic ICT Research Center, Network Research Institute. His research interests include microwave/millimeter-wave/terahertz photonics, ultrafast optical and radio communication systems, and ultrafast phenomena in semiconductor optical devices. He is a member of the Institute of Electronics, Information and Communication Engineers (IEICE), the Japan Society of Applied Physics (JSAP), and the International Society for Optics and Photonics (SPIE).

PHAM TIEN DAT (Member, IEEE) received the B.Eng. degree in electronics and telecommunication engineering from the Posts and Telecommunications Institute of Technology, Hanoi, Vietnam, in 2003, and the M.Sc. and Ph.D. degrees in science from Waseda University, Tokyo, Japan, in 2008 and 2011, respectively. In 2011, he joined the National Institute of Information and Communications Technology, Tokyo, Japan, where he is currently a Senior Researcher. His research interests include the fields of microwave/millimeter-wave photonics, radio over fiber, optical wireless systems, and seamless access networks for 5G and beyond.

KEIZO INAGAKI received the B.E. and M.E. degrees in electrical engineering from Kyoto University, in 1985 and 1987, respectively, and the D.E. degree from the Tokyo Institute of Technology, in 2011. In 1987, he joined ATR Optical and Radio Communications Research Laboratories, where he had engaged in the research and development of free space laser communication systems. Since April 2002, he moved ATR Wave Engineering Laboratories, where he joined the research project on optical gyroscope. Since December 2009, he has been with the National Institute of Information and Communications Technology, where he engaged in research and development of high precision measurement using advanced photonics technologies. He is a member of the Institute of Electronics, Information and Communication Engineers (IEICE).

KOSUKE TANABE received the master's degree in electrical engineering from the Science University of Tokyo, Japan, in 1993. He joined NEC Corporation, Japan, in 1993. Since joining the company, he has been engaged in the development of antenna systems for fixed wireless access systems and mobile base station. He is currently a Manager with the first Wireless Access Solutions Division, NEC. His research interests include antenna system for mobile backhaul, digital beamforming, and active antenna system for 5G base station.

EISAKU SASAKI (Member, IEEE) received the B.E. degree from Osaka University, Japan, in 1986. He joined NEC Corporation, Japan, in 1986. Since joining the company, he has been engaged in the development of microwave and millimeter-wave radios, which are used mainly as mobile backhaul system today. He is currently a Senior Professional with the first Wireless Access Solutions Division, NEC. His research interests include error-correcting codes, signal processing for higher-order modulation, and spatial multiplexing transmission systems, including OAM.

THOMAS KÜRNER received the Dipl.-Ing. degree in electrical engineering and the Dr.-Ing. degree from the University of Karlsruhe, Germany, in 1990 and 1993, respectively. From 1990 to 1994, he was with the Institut für Höchstfrequenztechnik und Elektronik (IHE), University of Karlsruhe, working on wave propagation modeling, radio channel characterization, and radio network planning. From 1994 to 2003, he was with the Radio Network Planning Department at the headquarters of the GSM 1800 and UMTS operator E-Plus Mobilfunk GmbH & Company KG, Düsseldorf, where he was the Team Manager of radio network planning support responsible for radio network planning tools, algorithms, processes, and parameters, from 1999 to 2003. Since 2003, he has been a Full University Professor of mobile radio systems with the Technische Universität Braunschweig. In 2012, he was a Guest Lecturer with Dublin City University within the Telecommunications Graduate Initiative in Ireland. He is currently the Chair of the IEEE 802.15 Standing Committee THz. He was also the chair of IEEE 802.15.3d TG 100G, which developed the worldwide first wireless communications standard operating at 300 GHz. He is also a Project Coordinator of the H2020-EU-Japan Project ThoR (TeraHertz end-to-end wireless systems supporting ultra-high data Rate applications) and a Coordinator of the German DFG-Research Unit FOR 2863 Meteracom (Metrology for THz Communications). In 2019, he received the Neal-Shephard Award of the IEEE Vehicular Technology Society (VTS). From 2016 to 2021, he has been a member of the Board of Directors of the European Association on Antennas and Propagation (EurAAP), and since 2020, he is a Distinguished Lecturer of IEEE Vehicular Technology Society.

BO KUM JUNG received the B.E. degree from Inha University, Incheon, South Korea, in 2015, and the M.Sc. degree from the Technische Universität Braunschweig, Braunschweig, Germany, in 2019, where he is currently pursuing the Ph.D. degree. His current research focuses on the THz communication systems, wave propagation at THz frequency spectrum range, and THz wireless backhaul/fronthaul.

TETSUYA KAWANISHI (Fellow, IEEE) received the B.E., M.E., and Ph.D. degrees in electronics from Kyoto University, Kyoto, Japan, in 1992, 1994, and 1997, respectively. From 1994 to 1995, he was with the Production Engineering Laboratory, Panasonic. In 1997, he was with the Venture Business Laboratory, Kyoto University, where he was engaged in research on electromagnetic scattering and near-field optics. In 1998, he joined the Communications Research Laboratory, Ministry of Posts and Telecommunications (now the National Institute of Information and Communications Technology), Tokyo, Japan. In 2004, he was a Visiting Scholar with the Department of Electrical and Computer Engineering, University of California at San Diego. Since April 2015, he has been a Professor with Waseda University, Tokyo. His current research interests include high-speed optical modulators and RF photonics.